Korean J. Chem. Eng., 35(8), 1700-1709 (2018)
DOI: 10.1007/s11814-018-0079-8

pISSN: 0256-1115
eISSN: 1975-7220

Interfacial polymerization of facilitated transport polyamide membrane prepared from PIP and IPC for gas separation applications

Abdelrahman Awad* **and Isam H. Aljundi*,**,†**

*Chemical Engineering Department, King Fahd University of Petroleum and Minerals, Dhahran 31261, Saudi Arabia
**Center of Excellence in Nanotechnology, King Fahd University of Petroleum and Minerals, Dhahran 31261, Saudi Arabia
(*Received 7 February 2018 • accepted 10 May 2018*)

Abstract−A facilitated transport polyamide (PA) membrane was developed for gas separation by interfacial polymerization reaction of piperazine (PIP) and isophthaloyl chloride (IPC) supported on polysulfone (PSF) membrane previously prepared by dry/wet phase inversion method. The properties of the prepared membranes were characterized by SEM, FT-IR, TGA, and XRD. SEM images showed that a defect-free PSF, and rough PA membranes were fabricated, while the FT-IR spectra confirmed the formation of PA layer on top of the PSF support. The separation performance of the thin film PA and PSF membranes was evaluated using four gasses (CO_2, CH_4, N_2, and O_2). Compared to the PSF membrane, the PA membrane demonstrated an increased selectivity of CO_2/CH_4 and CO_2/N_2 by 178%, 169%, respectively. This improvement was attributed to the presence of amine functional groups, which acted as a fixed carrier to facilitate the transport of CO_2 gas across the membrane. However, building the PA layer on top of PSF support reduced the membrane permeance of CO_2 from 2.41 to 2.12 GPU as a result of the increased mass transfer resistance. Furthermore, the effect of operating temperature and pressure on the separation performance of the membranes was investigated.

Keywords: Polyamide, CO_2 Capture, Membrane, Gas Separation Natural Gas

INTRODUCTION

CO_2 emission can be considered as the primary source of global warming [1-3], which leads to extremely fluctuating weather and a damaged natural ecosystem [3]. The demand for a clean, green and safe source of energy is a critical concern for scientists, environmentalists, and environmental policy makers [4,5]. Currently, natural gas is considered as a potential alternative source of energy to meet the increasing demand for energy resources that are economically viable, and environmentally sustainable [6,7]. In the gas stream, carbon dioxide reduces the calorific value of the gas and affects the selling price. Furthermore, in presence of water, the gas stream becomes acidic and corrosive, which damages pipelines and equipment [8]. On the other hand, CO_2 separation could produce a highly concentrated CO_2 stream that can be used in enhanced oil recovery after its removal from the natural gas stream and in other chemical industries rather than direct release into the atmosphere [9]. Therefore, CO_2 removal from natural gas has the synergistic effect of controlling the greenhouse gas emissions in addition to the economic benefits. CO_2 separation can be achieved using absorption, adsorption, cryogenic, or membrane processes where each of these processes has its own advantages and drawbacks [10,11]. Among which, the absorption process is the most developed commercial technology. However, the cost of energy for solvent regeneration, corrosion of the equipment and flow problems are serious problems in this process [6]. Alternatively, membrane technology has shown enormous potential for the application of gas separation [12,13]. Unlike all other technologies, there is no need for phase transformation. Besides, the advantages of equipment simplicity, ease of scale-up, and small footprint make membrane technology an attractive option for the industry. However, CO_2 capture from natural gas using efficient and robust membrane is still one of the challenges in membrane-based gas separation [4,9].

CO_2 removal using facilitated transport membranes has been recognized as one of the routes to enhance the performance of organic membranes in order to provide efficient gas separation. CO_2 transport mechanism in membranes containing amine functional groups (primary or secondary) can be expressed by the following equations [14]:

$$2RNH_2+2CO_2 \longleftrightarrow RHNCOOH+RNH_3^+ \quad (1)$$

$$2R_2NH+2CO_2 \longleftrightarrow R_2NCOOH+R_2NH_2^+ \quad (2)$$

In these reactions, CO_2 reacts rapidly with the primary or secondary amine-carrier to produce RNHCOO- in the membrane. Moreover, some researchers suggested that in presence of water, tertiary amines can act as a catalyst and react with CO_2 as follows [15]:

$$R_3N+CO_2+H_2O \longleftrightarrow R_3NH^++HCO_3^- \quad (3)$$

In addition to promoting ion transfer in the hydration reaction (Eq. (3)), the wet condition of membranes can enhance the chain mobility of the polymer matrix, and hence higher gas diffusion is expected [14]. Compared to primary and secondary amine groups, tertiary amines revealed better gas absorption capacity, higher catalytic efficiency in the hydration reaction, more stability in air, and lower crystallinity [15]. Facilitated transport composite-membranes are generally fabricated using solution coating [16,17], plasma polymerization [18,19], dry/wet phase inversion [20-22] and interfacial

†To whom correspondence should be addressed.
E-mail: aljundi@kfupm.edu.sa, isam.aljundi@yahoo.com

polymerization (IP) techniques. The latter technique can be defined as a type of step-growth polymerization in which polymerization reaction occurs at the interface between an aqueous solution containing one monomer (polyamine) and an organic solution containing a second monomer (polyacyl halides) [5]. Commercial membranes fabricated using IP are available as fhin film composite for reverse osmosis [23,24], nanofiltration [25,26], and pervaporation process [27]. These membranes have the possibility of producing ultrathin skin layer (0.1-1.0 μm), the availability of a large number of monomers that can be used, and more importantly the defect-free nature and ease of scale-up to the commercial modules [4]. However, thin film composite membranes fabricated using IP for the application of gas separation still lag behind and need more studies.

The formation and separation performance of PA membranes are greatly affected by selecting the proper monomer for IP reaction. Distinctive membrane morphologies and thicknesses were observed due to the differences of the amine monomer solution in terms of solubility and reactivity in the organic phase [28]. Such distinctive properties will dramatically affect the membrane chemical and physical properties, including the permeance and selectivity. Sridhar et al. [29] investigated the performance of interfacially polymerized PA membrane fabricated from m-phenylenediamine (MPD) and IPC using PSF support. The results showed a CO_2 permeance of 15.2 GPU with a CO_2/CH_4 selectivity of 14.4, while the H_2S permeance was 51.6 GPU with H_2S/CH_4 selectivity of 49.1. Xingwei et al. [15] prepared PA membrane using DNMDAm and TMC on PSF membrane as a support. The gas permeation tests using 20/80 v/v feed gas of CO_2/N_2 demonstrated a CO_2 permeance of 173 GPU and CO_2/N_2 selectivity of 70 at a feed pressure of 0.11 MPa. When the gas mixture was changed to 10/90 v/v, the permeance and selectivity dropped down to 118 GPU and 37, respectively.

Piperazine is a cyclic diamine used extensively in activated amine solutions for CO_2 absorption. It has two secondary amino groups and has a high CO_2 reaction rate constant [30]. It is used in fabrication of nanofiltration membranes for liquid separation; however, to the best of our knowledge, it has never been used as a monomer to fabricate PA composite membrane for gas separation. Therefore, our aim was to develop a new PIP-derived facilitated transport membrane for the application of gas separation. A series of characterization techniques (SEM, FT-IR, XRD, and TGA) were used to study the merits of the new membrane. The separation performance of the fabricated membrane was evaluated by testing the permeation with different gasses (CO_2, O_2, N_2, and CH_4).

MATERIALS AND METHODS

1. Materials

All chemicals were purchased from Sigma-Aldrich, except methanol and n-hexane from Scharlau. Polysulfone pellets (Mw of 35000) were used to fabricate the membrane support. *N,N*-dimethylacetamide (DMAC) with a purity of 99.9% was used as a less volatile solvent, inhibitor-free tetrahydrofuran (THF) with a purity of 99.9% was the primary volatile solvent, while absolute ethanol was selected as a non-solvent additive. PIP and IPC with a purity of 99% were used as the monomers for the IP reaction.

Table 1. Composition and amount of the dope solution

Component	Amount (g)	Concentration (%)
PSF pellets	4.00	23.03
DMAC	5.81	33.45
THF	5.81	33.45
Ethanol	1.75	10.07

2. Membrane Preparation

2-1. Polysulfone Support

PSF support was fabricated by the dry/wet phase inversion technique. Prior to membrane preparation, the PSF polymer particles were dried overnight at 100 °C in a vacuum oven to completely remove the moisture from the polymer. Dry PSF pellets were dissolved in a mixture of DMAC and THF, then ethanol was added and the solution was stirred for 24 h at 25 °C with a magnetic stirrer. The polymeric solution (Table 1) was degassed at room temperature for 24 h to remove air bubble. The solution was cast on a clean glass plate with a thickness of 200 μm using a casting knife. The membrane was left in air for 60 s at ambient condition and subsequently immersed in a de-ionized (DI) water bath for 24 h. The prepared membranes were immersed in methanol for 2 h for solvent-exchange and treated with Polydimethylsiloxane (3% in hexane) to eliminate infinitesimal defects or pinholes in the membrane and then finally dried in vacuum oven at 100 °C for 48 h.

2-2. Polyamide Membrane

PA membrane was prepared using IP method in which polymerization reaction occurs between PIP (in DI water) and IPC (in hexane) as shown in Fig. 1. The previously prepared PSF support was saturated with PIP solution (2%w/v) for ten minutes, then a rubber roller was used to remove the excess PIP solution. The support was immersed in the organic solution (0.2%w/v IPC) for 3 minutes and the excess unreacted IPC was removed using pure hexane. Finally, the membrane was dried at 80 °C for 10 min and the fabricated PA membranes were kept in DI water.

3. Membrane Characterization

Fourier transformation infrared spectrometer (FT-IR, Nicolet 6700, Thermo Electron Corporation) was used to investigate the chemical structure of the fabricated PA composite layer. Scanning electron microscope (SEM, MIRA 3, Tescan) images were taken to

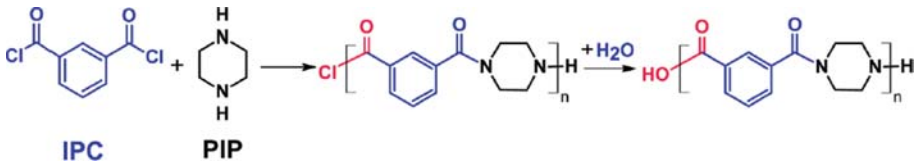

Fig. 1. Polymerization reaction between PIP and IPC [31].

study the surface morphology of the prepared membranes. Membrane samples were coated with 5 nm gold layer prior to SEM analysis using Ion sputter coater (Q150R S, Quorum Technologies). Analysis by X-ray diffraction (XRD, D8-Advance, Bruker) of the prepared PA membranes was performed to get information about the crystallinity. Furthermore, thermal stability of fabricated composite membrane was examined by thermogravimetric analysis (TGA, STA 449 F3 Jupiter, Netzsch) in the temperature range of 30-800 °C at 10 °C/min heating rate under nitrogen flow of 100 mL/min.

4. Gas Permeation Measurements

The permeability of the fabricated PSF and PA membranes was examined using four pure gases (CO_2, N_2, O_2, and CH_4). The membranes were tested at a feed pressure from (1-5 bar) and at different temperatures (300.15, 308.15, and 323.15 K). The gas permeation experiments were conducted using the well-known constant volume/variable pressure (time-lag) method [32-34]. As shown in Fig. 2, the gas permeation setup was built to work in two modes (constant volume/variable pressure and constant pressure/variable volume). The system contains three Bronkhost Coriolis mass flow controllers, membrane module, a permeation volume, a vacuum pump that is connected to the permeate volume through a valve, and pressure transducers to detect the feed and permeate pressures. The process is controlled by a software and the data is collected by LabVIEW. A membrane sample with an effective area of 4.91 cm^2 was cut and fixed inside the membrane cell, and both sides of the membrane module were evacuated. The gas was then fed into the module at a constant pressure. To determine the gas permeation, the valve used for the evacuation was closed and the pressure change in the permeate side was monitored with time. The leak rate was measured at the start of each experiment to get accurate permeation rate, and the data reported here is the average of at least two independent measurements. The permeance (p) was calculated in gas permeation units (1 GPU=10^{-6} cm^3 (STP)/(s cm^2 cm-Hg)) using Eq. (4) [35]:

$$p=\frac{273.15\times10^{6}\,V_d}{760\left(P_2\times\frac{76}{14.7}\right)A\,T}\left[\left(\frac{dP_1}{dt}\right)_{ss}-\left(\frac{dP_1}{dt}\right)_{leak}\right] \quad (4)$$

where V_d is the downstream volume (cm^3), A is the effective membrane area (cm^2), P_2 is the upstream pressure (psi), and $(dP_1/dt)_{ss}$ is the rate of pressure change in the downstream chamber at the steady state in mmHg/s, and $(dP_1/dt)_{leak}$ is the leak rate in mmHg/s, T is the cell temperature in K. The selectivity of gas i to j (α_{ij}) was estimated by Eq. (5):

$$\alpha_{ij}=p_i/p_j \quad (5)$$

RESULTS AND DISCUSSION

1. Membrane Characterization

To confirm the formation of the PA layer on the PSF support membrane, SEM analysis for both PSF and PA membranes was carried out as shown in Fig. 3. It was observed that PSF membrane has a smooth top surface compared to the rough PA and it has an asymmetric structure with a dense top layer. It is believed that the asymmetric structure resulted from the phase separation along with the instantaneous de-mixing in a quaternary system (polymer, solvent, nonsolvent, and an additive) because DMAC solvent has high mutual affinity for water and the dense layer was built as a result of the dry step before coagulating the membrane in the water bath [36-39]. During the initial step of dry inversion process, THF was removed from the surface of the dope solution because it has the lowest boiling point (65.48 °C). For the PA surface, SEM images showed that a defect-free PA layer was built on top of the PSF layer and the smooth PSF surface was totally covered by a rough film of PA structure. This layer was formed as a result of IP reaction be-

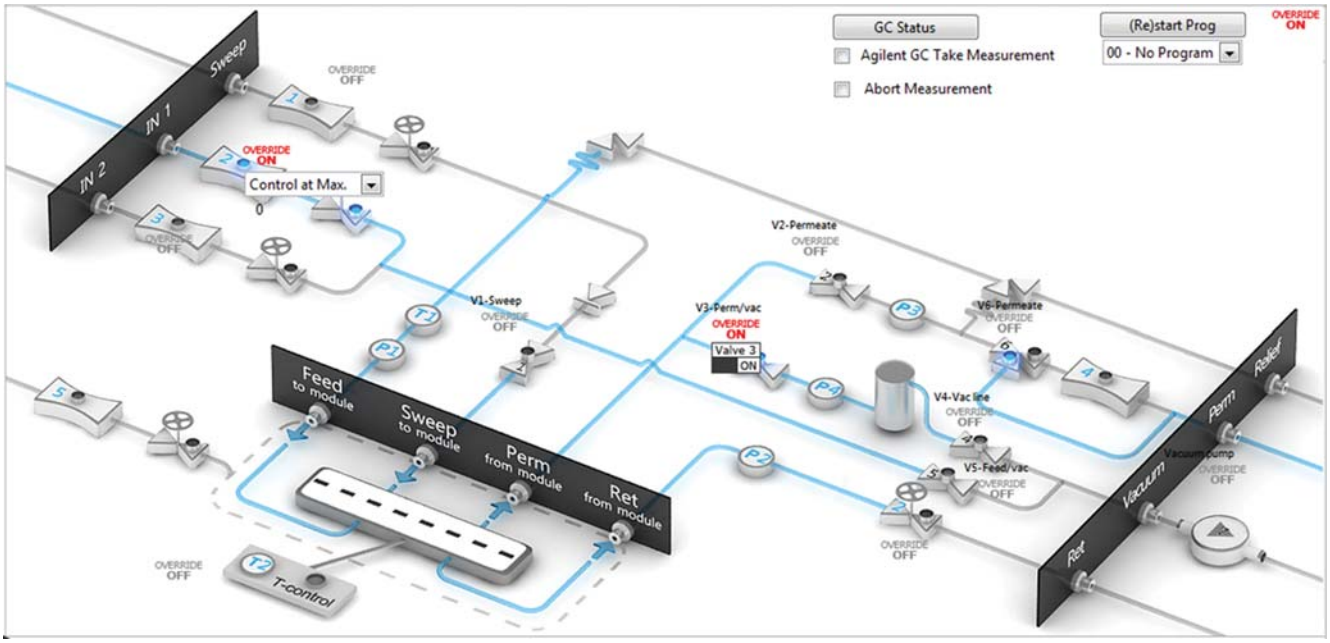

Fig. 2. Flowsheet of the setup used in the permeation experiments.

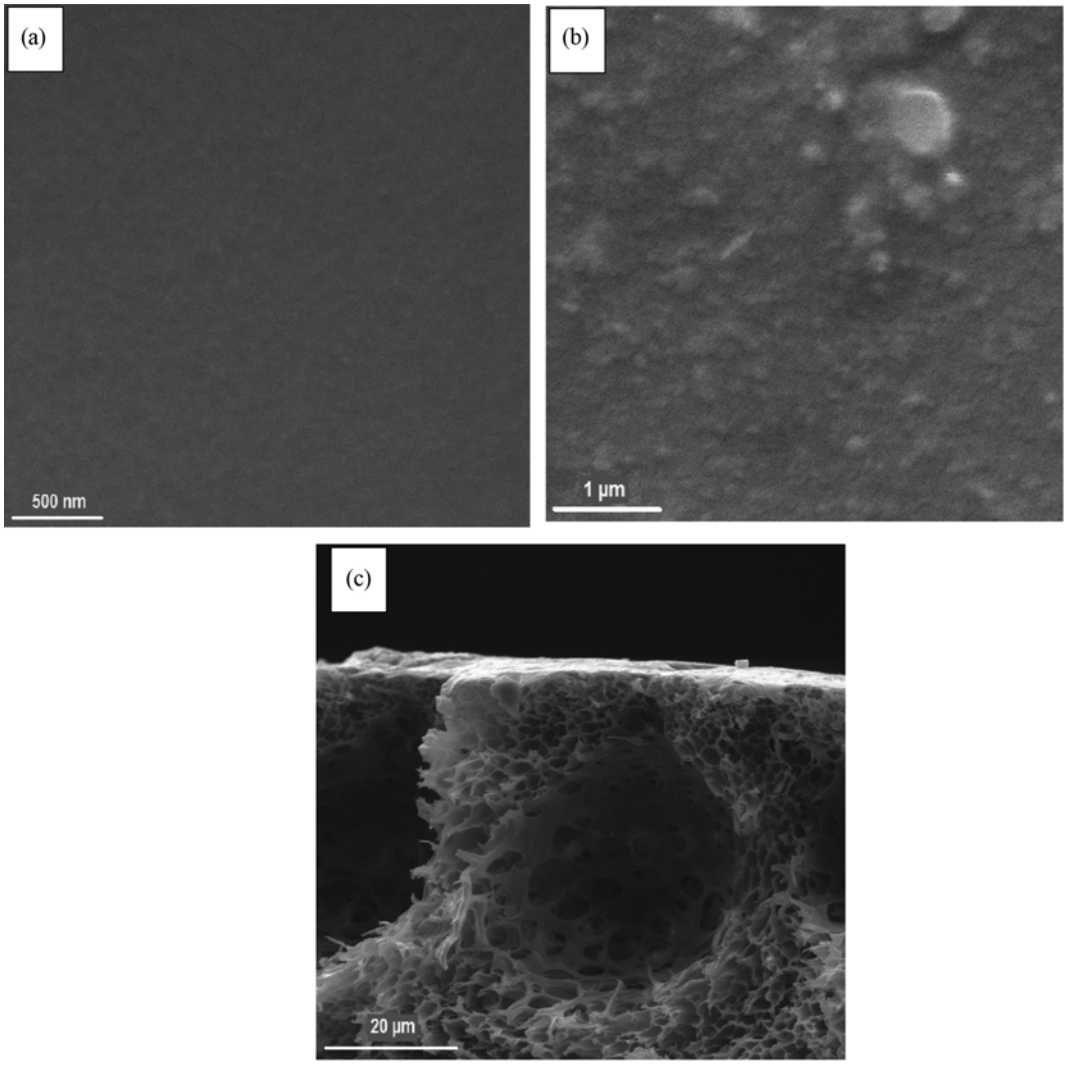

Fig. 3. SEM images of (a) surface of PSF support, (b) surface of PA membrane, and (d) cross section of the PA membrane on top of the PSF support.

tween PIP and IPC. When the PIP diffusivity is considerably higher than the PIP solubility in the organic phase (hexane), the amine will react strongly with the acid chloride to produce a dense PA film, which brings the reaction to self-termination. On the contarary, solvent with greater amin solubilty results in thick but less crosslinked form. Moreover, the highlty crosslinked film will tie the polymer chains together and hamper the PA chain mobility that promotes CO_2 induced plasticization resistance [40,41].

FTIR spectra of the PA composite layer were scanned in the range of 400 cm^{-1} to 4,000 cm^{-1} to study the chemical composition of the membrane. The bands are ascribable for the interfacially polymerized layer as well as PSF support skin because the depth of the beam penetration is thicker than PA layer [7]. The band at 1,680 cm^{-1} shown in Fig. 4 is ascribed to the amide I (C=O) stretch, whereas the broadband at 1,590 cm^{-1} is attributed to amide II (C-N) stretch. Moreover, a band of the amine group (NH stretch) was observed at a wavelength of 1,500 cm^{-1}. Therefore, the existence of amide I and II in the FT-IR spectra confirmed the formation of the PA layer as a result of the IP reaction.

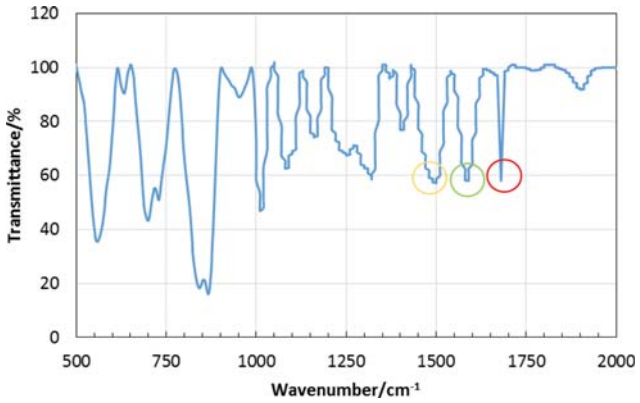

Fig. 4. FTIR spectrum of the PA membrane.

The thermal behavior of the fabricated PA membrane was studied by TGA test as shown in Fig. 5. Nearly 5-6 mg of the fabricated membrane was heated at a constant heating rate of 10 °C/min from

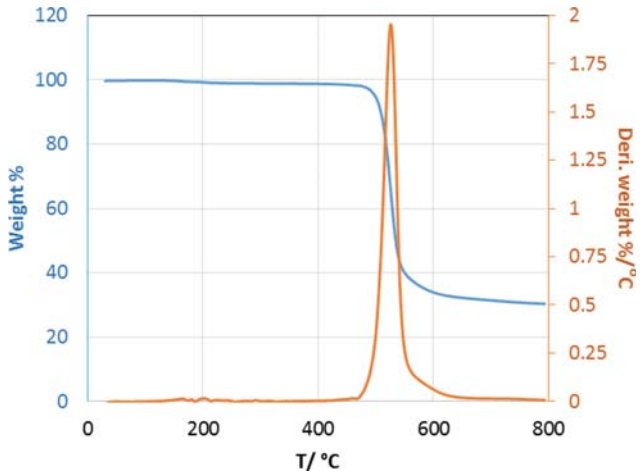

Fig. 5. TGA and DTG curves of the PA membrane.

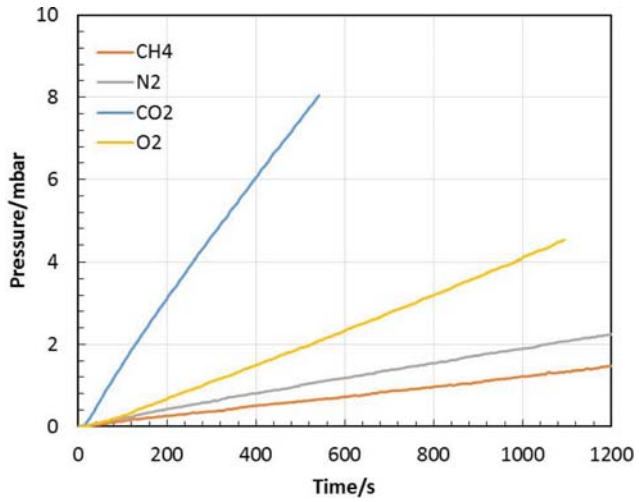

Fig. 7. The time-lag behavior of the tested gases using PA membrane.

room temperature to 800 °C under inert N_2 atmosphere with a flow rate of 100 mL/min. It was observed that no considerable weight loss occurred up to a temperature of 480 °C, which is comparable to the thermal stability of other prepared PA reported in the literature [42]. However, the membrane started to lose weight significantly at approximately 490 °C as the weight reduced to 33.0% at a temperature of 600 °C. The thermal stability could be evaluated better in terms of $T_{d5\%}$, $T_{d10\%}$, and $T_{d50\%}$ values (the temperatures at which the tested membrane loses 5, 10, and 50% of its initial mass), respectively. The TGA data showed that the value of $T_{d5\%}$, $T_{d10\%}$, and $T_{d50\%}$ occurred at a temperature of 498 °C, 508 °C, and 534 °C; respectively.

Bruker D8-Advance X-ray diffractometer was used to take XRD spectra of PSF and the composite PA membranes with a wavelength of 1.5414 Å. The angle of diffraction (2θ) was changed from 5° to 50° to observe the nature of the membrane structures. A scanning rate of 2°/min operating at 30 kV and 30 mA was used for XRD spectra. As shown in the XRD spectra of both PA and PSF membranes (Fig. 6), the peak centered around 19° revealed an amorphous structure [43]. While for the PA membrane, the relatively sharp peak around 21° indicates the semi-crystalline nature of composite thin layer. The presence of crystalline regions can be attributed to the thin PA layer, while amorphous regions appeared as results of PSF structure [29].

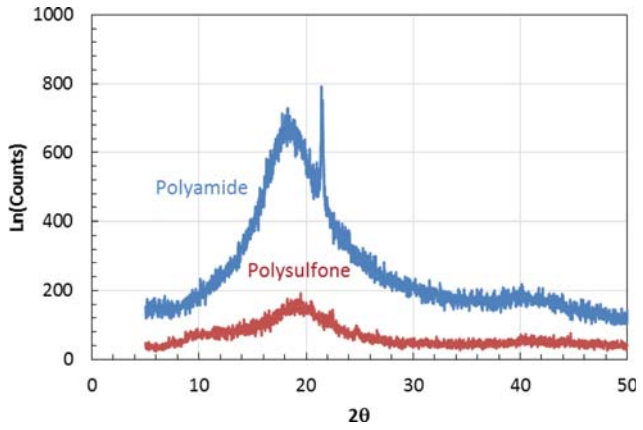

Fig. 6. XRD pattern for the PSF and PA.

2. Gas Permeation Properties

2-1. Time-lag Behavior of the Tested Membranes

Fig. 7 and 8 shows the time-lag behavior of each gas using both membranes. In both cases, the permeation of CO_2 was much faster than the other gases followed by the oxygen. However, the methane and nitrogen had a comparable permeation rate. It is known that the amide and free amine groups in PA membrane render the facilitated transport mechanism of CO_2 and these functional groups are activated in the presence of moisture on the surface [44]. Our membrane samples were saturated by DI water before testing the gases to benefit from the facilitated transport mechanism of CO_2. Therefore, we believe that the fast permeation of CO_2 can be explained by both the facilitated transport and the solution diffusion mechanisms.

Table 2 represents the separation performance of both PA and

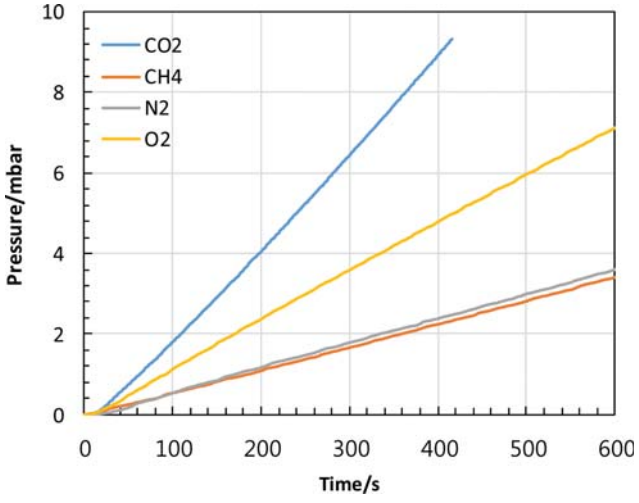

Fig. 8. The time-lag behavior of the tested gases using PSF membrane.

Table 2. Gas permeation measurements of PA and PSF membrane at 300.15 K and 5 bar

	Permeance (GPU)				Selectivity		
Membrane	CO_2	CH_4	N_2	O_2	CO_2/CH_4	CO_2/N_2	O_2/N_2
Polyamide	2.124	0.175	0.182	0.438	12.07	11.64	2.40
Polysulfone	2.411	0.556	0.557	1.196	4.336	4.325	2.146

PSF membranes at 300.15 K and a feed pressure of 5 bar. It can be observed that the ideal gas selectivities of PSF membrane were enhanced by building the thin film PA layer, while the gas permeance decreased as a result of the increased mass transfer resistance. Moreover, the CO_2 was the fastest moving gas with a permeance of 2.12 and 2.41 GPU for PA and PSF membranes, respectively. Oxygen was the second in permeance with 0.438 and 1.196 GPU for PA and PSF membranes, respectively. As a whole, the gas permeation of the prepared composite PA membrane as well as PSF membrane followed the order of kinetic diameters of the gasses used in these experiments. Since the order of gas permeance was CO_2> O_2>N_2>CH_4, and the kinetic diameters of gas molecules are 0.330 nm for CO_2, 0.346 nm for O_2, 0.364 nm for N_2, and 0.380 nm for CH_4.

The improved separation performance of PA membrane was mainly attributed to the presence of amide and amine groups in the thin film composite membrane. Since CO_2 is a soluble gas, it is believed that it undergoes dissolution in PA layer, which contains polar -NHCO functional groups [14,45]. Furthermore, CO_2 molecules are expected to form hydrogen bonding interactions with amide groups from the PA membrane. Whereas, the saturated nonpolar CH_4 and N_2 gas molecules exhibited poor interaction with the membrane and hence showed much lower permeance. In addition, a reversible reaction between amine groups and CO_2 molecules is expected to occur in wet PA membrane, which produces complex and HCO_3^- components that could diffuse freely across the membranes [15]. However, because methane and nitrogen did not react with the PA film, their transport across the membrane is based on simple solution-diffusion mechanism. As a result, relativity high selectivity of CO_2/CH_4 and CO_2/N_2 gas pairs was recorded for the fabricated TFC membranes as shown in Table 2. These selectivities were one order of magnitude higher than that of the PSF membrane. Even for the O_2/N_2 gas pair, the selectivity was enhanced about 12% in the PA membrane.

2-2. Effect of Operating Temperature

The effect of operating temperature on the membrane performance was investigated at a temperature range from 300.15 to 323.15 K with the four pure gases as shown in Table 3. The temperature dependence of gas permeance can be expressed by the Arrhenius equation as follows [46]:

$$p=p_o \exp(-E/RT) \quad (6)$$

Generally speaking for polymeric membranes, increasing the operating temperature results in higher free volume for gas molecules to transport and more flexible polymer chains. This will lead to higher gas diffusion and permeation. At the same time, lower pair gas selectivity is expected by increasing the temperature as a result of the wider polymer chain motions and more loose structure of the membrane [47]. From Table 3, the permeance of all gases was enhanced with increasing the operating temperature. Nevertheless, the permeation improvement was not the same for all gasses. For instance, by increasing the operating temperature from 300.15 to 323.15 K, the PA membrane permeance of CO_2 increased by 32.1%, while the CH_4 permeance increased by 71.7%. Moreover, N_2 and O_2 gas permeances improved by 73.0% and 49.1%, respectively. The reason behind the much higher increase in the permeance of CH_4, N_2, and O_2 gases compared to CO_2 is that the permeation of these gases is based on simple molecule diffusion, while CO_2 gas has strong interaction with the PA functional groups, which results in higher solubility [32,47]. The gas solubility is reduced with increasing the temperature, and the reduction is higher for the more condensable gas (CO_2) compared with O_2, N_2, and CH_4 gases. For PSF membrane, the CO_2 permeance improved by 17.95% as the temperature increased from 300.15 to 323.15 K, while the gas permeance ncreased by 51.1%, 44.5%, and 28.3% for CH_4, N_2, and O_2; respectively.

Table 3. Separation performance of PSF and PA membranes at different temperatures and 5 bar

	Permeance (GPU)				Selectivity		
				Polysulfone			
T(K)	CO_2	CH_4	N_2	O_2	CO_2/CH_4	CO_2/N_2	O_2/N_2
300.15	2.411	0.556	0.557	1.196	4.336	4.325	2.146
308.15	2.450	0.604	0.622	1.312	4.051	3.939	2.109
323.15	2.844	0.840	0.805	1.535	3.383	3.531	1.906
				Polyamide			
300.15	2.124	0.175	0.182	0.438	12.07	11.64	2.40
308.15	2.449	0.221	0.256	0.579	11.07	9.54	2.25
323.15	2.806	0.301	0.315	0.653	9.29	8.88	2.07

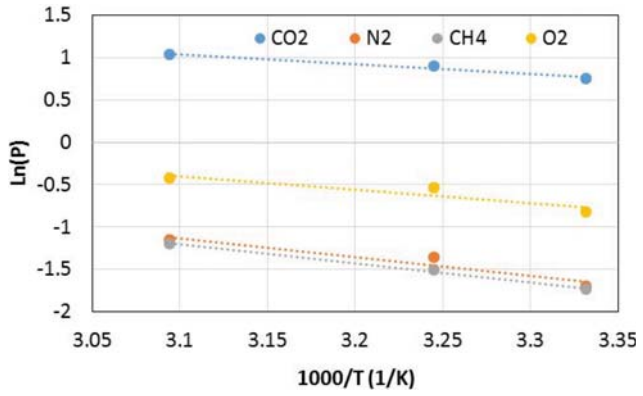

Fig. 9. The effect of temperature on the gas permeance for PA membrane.

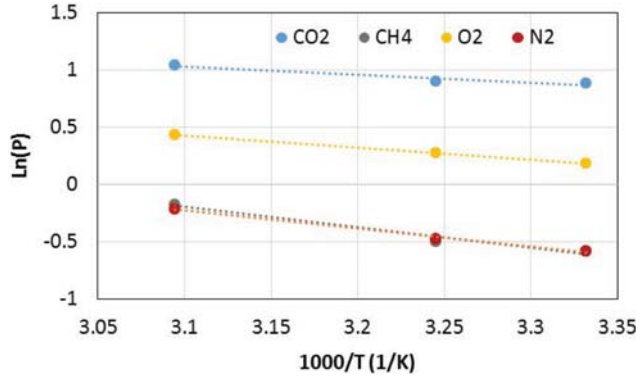

Fig. 10. The effect of temperature on the gas permeance for PSF membrane.

The general trend shows that there is a decrease in the selectivity with the increase in the operating temperature. This can be explained by the significant increase in the permeance of all gases compared to that of the CO_2.

The natural logarithm of the permeance, ln(p), was plotted against 1/T to calculate the activation energy from the solpe of the straight line, as shown in Fig. 9 and 10. The values of the activation energies for all gasses in both membranes are tabulated in Table 4. For PA membrane, the values of the activation energy followed the permeance order in which $E_{CO2}<E_{O2}<E_{N2}<E_{CH4}$. The activation energy is generally affected by the gas/polymer interaction as well as the molecular size of the penetrant. In addition, gases with lower activation energies move faster through the membrane and vice versa [46]. From the literature [47], the low activation energy of CO_2 can be attributed to the high gas solubility in the PA. Similar observations were reported for polyimide, polyarylene ether, and cellulose membranes [48,49].

Table 4. Activation energies of (CO_2, CH_4, N_2, and O_2) for PA and PSF membranes

Membrane	E_{CO2} (kJ/mol)	E_{CH4} (kJ/mol)	E_{N2} (kJ/mol)	E_{O2} (kJ/mol)
Polyamide	9.509	18.754	18.355	13.192
Polysulfone	6.061	14.897	13.052	8.730

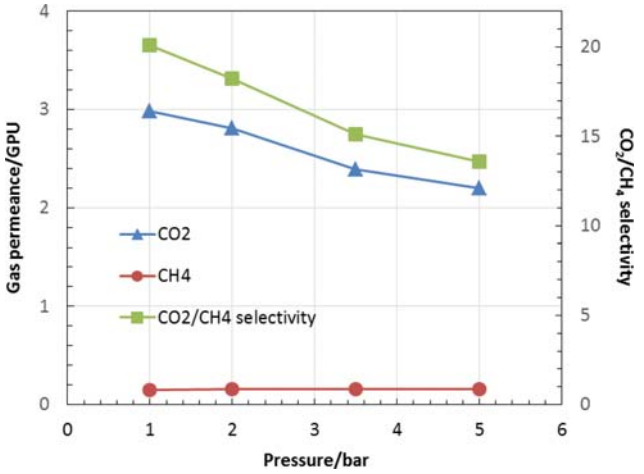

Fig. 11. The pressure effect of feed gases (CO_2, CH_4) on permeance and selectivity for the PA membrane.

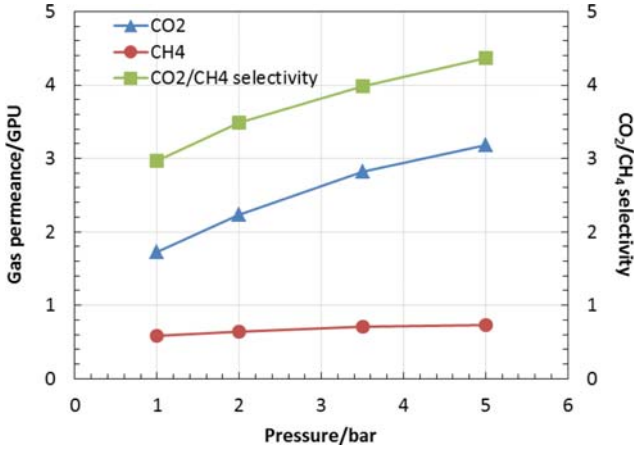

Fig. 12. The pressure effect feed gas (CO_2, CH_4) on permeance and selectivity for PSF membrane.

2-3. Effect of Feed Pressure

To investigate the effect of feed gas pressure on the separation performance of both membranes, different pressures were applied at a constant temperature of 300.15 K, and the results are illustrated in Figs. 11-14. It can be seen that the PA membrane-permeance for CO_2 decreased with increasing feed pressure (Fig. 11), while for the PSF membrane, CO_2 permeance increased slightly (Fig. 12). For example, when the feed pressure increased from 1 to 5 bar, PA membrane-permeance for CO_2 declined 28.62%, while the PSF membrane-permeance of CO_2 was enhanced 83.92%.

It is known that CO_2 reacts with the amide group (according to Eq. (3)) in PA membranes to produce a complex and HCO_3^- which can diffuse from one site to another. Therefore, by increasing the CO_2 amount within the membrane, amine carriers might reach the saturation state and cannot combine with other CO_2 molecules anymore, thereby lower CO_2 permeance is expected from this mechanism of permeation [50,51]. However, the enhanced CO_2 permeance in the PSF membrane is attributed to the higher molecu-

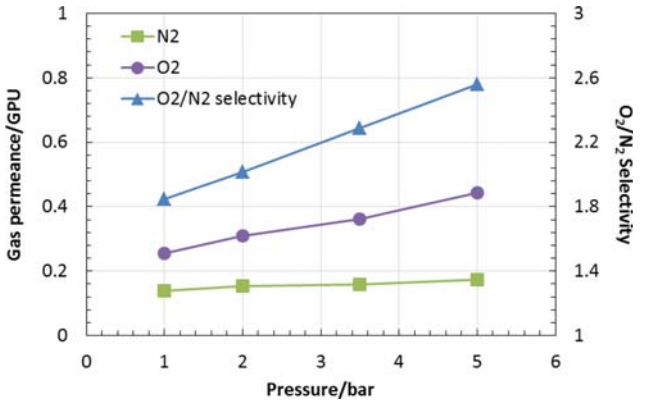

Fig. 13. The pressure effect of feed gas (O_2, N_2) on the permeance and selectivity for the PA membrane.

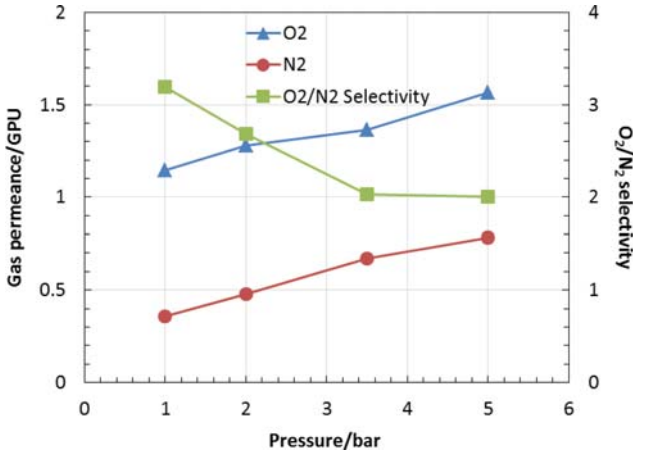

Fig. 14. The pressure effect of feed gas (O_2, N_2) on permeance and selectivity for PSF membrane.

lar concentration of CO_2 at the gas membrane interface, which will increase the driving force and results in higher gas permeation.

On the other hand, the PA membrane-permeance of methane was almost constant when the feed pressure increased from 1 to 5 bar. Since CH_4 molecules do not react with PA membrane, the transport of methane gas across the membrane is based on simple solution-diffusion mechanism. As a result of the decreased CO_2 permeance with increased feed pressure (while almost constant CH_4 permeance was maintained), CO_2/CH_4 selectivity declined with pressure [35,52]. However, higher feed pressure resulted in higher molecular concentration at the PSF membrane/gas interface, which caused CO_2 and CH_4 permeance to increase.

The gas transport behavior of oxygen and nitrogen in the PA and PSF membranes is shown in Figs. 13-14. The transport of these gasses is based on the solution-diffusion mechanism. Hence, at higher pressure, gas concentration at the membrane interface increased, which offered higher driving force for mass transfer of O_2 and N_2 gases. The oxygen permeance in the PA membrane (Fig. 13) was enhanced by 74.1% when the feed pressure was increased from 1 to 5 bar, while the nitrogen permeance improved by 25.54%. The high increase in O_2 permeance compared to the nitrogen gas caused the gas pair (O_2/N_2) selectivity to improve by 38.6%. The PSF membrane experienced 36.7% and 117% increase in O_2 and N_2 permeance, respectively, while O_2/N_2 selectivity declined 37.2% as the feed pressure increased from1 to 5 bar (Fig. 14).

CONCLUSIONS

PA composite membrane was successfully fabricated by IP reaction of PIP and IPC using PSF as a support. The characterzation tests confirmed the formation of a rough PA structure on top of a smooth PSF membrane. Moreover, XRD pattern of TFC membrane showed both crystalline regions (attributed to the PA layer) and amorphous regions (resulting from PSF structure). The gas permeation measurements suggested that CO_2 reacted reversibly with amine functional groups of the PA, which facilitated the transport of CO_2 through the membrane with a relatively high CO_2/CH_4 and CO_2/N_2 selectivities. The permeance of the tested gase increased with the operating temperature, whereas the gas selectivity decreased as a result of the wider polymer chain motion as well as the looser structure at high temperature.

ACKNOWLEDGEMENT

The authors would like to acknowledge the support provided by King Abdulaziz City for Science and Technology through NSTIP for funding this work under project No. 14-ADV303-04.

NOMENCLATURE

Acronyms

PSF : polysulfone
PA : polyamide
GPU : gas permeation units
IP : interfacial polymerization
DMACs : *N, N*-dimethylacetamide
THF : tetrahydrofuran
DI : deionized water
IPC : isophthaloyl chloride
PIP : piprazine
TMC : trimesoyl chloride
MPD : m-phenylenediamine
FT-IR : fourier transformation infrared
XRD : x-ray diffraction
TGA : thermogravimetric analysis
SEM : scanning electron microscopy

Variables

T : cell temperature [K]
R : universal gas constant [kJ/K·kmol]
E : apparent activation energy for gase permeation [kJ/mol]
P_2 : the upstream pressure [kPa]
A : effective membrane area [cm^2]
V_d : downstream volume [cm^3]

Greek Letter

p : gas permeance [GPU]

p_o : pre-exponential coefficient
α_{ij} : gas selectivity

REFERENCES

1. J. Adewole, A. Ahmad, S. Ismail and C. Leo, *Int. J. Greenh. Gas Control.*, **17**, 46 (2013).
2. P. Shao, M. Dal-Cin, M. Guiver and A. Kumar, *J. Membr. Sci.*, **427**, 451 (2013).
3. J. Leggett, R. Lattanzio, C. Ek and L. Parker, An Overview of Greenhouse Gas (GHG) Control Policies in Various Countries, Congressional Research Service (2009).
4. K. Wong, P. Goh and A. Ismail, *J. Mater. Chem. A Mater. Energy Sustain.*, **4**, 15726 (2016).
5. K. Schoots, R. Rivera-tinoco, G. Verbong and B. Van Der Zwaan, *Int. J. Greenh. Gas Control.*, **5**, 1614 (2011).
6. T. Rufford, S. Smart, G. Watson, B. Graham, J. Boxall, J. C. Diniz and E. F. May, *J. Pet. Sci. Eng.*, **94**, 123 (2012).
7. M. Wang, W. Zhi, S. Li, C. Zhang, J. Wang and S. Wang, *Energy Environ. Sci.*, **6**, 539 (2013).
8. B. Shimekit and H. Mukhtar, Natural Gas Purification Technologies Major Advances for CO_2 Separation and Future Directions, Advances in Natural Gas Technology, H. Al-Megren, Eds., InTech, Croatia, 235 (2012).
9. M. Rezakazemi and A. Ebadi, *Prog. Polym. Sci.*, **39**, 817 (2014).
10. Y. Zhang, J. Sunarso, S. Liu and R. Wang, *Int. J. Greenh. Gas Control.*, **12**, 84 (2013).
11. L. Peters, A. Hussain, M. Follmann, T. Melin and M. Hägg, *Chem. Eng. J.*, **172**, 952 (2011).
12. R. Baker and K. Lokhandwala, *Ind. Eng. Chem. Res.*, **47**, 2109 (2008).
13. M. A. Aroon and A. F. Ismail, *Sep. Purif. Technol.*, **75**, 229 (2010).
14. J. Zhao, Z. Wang, J. Wang and S. Wang, *J. Membr. Sci.*, **283**, 346 (2006).
15. X. Yu, Z. Wang, Z. Wei, S. Yuan and J. Zhao, *J. Membr. Sci.*, **362**, 265 (2010).
16. M. Yoshikawa, K. Fujimoto, H. Kinugawa, T. Kitao and N. Ogata, *Chem. Lett.*, **23**, 243 (1994).
17. S. Du, X. Feng and A. Chakma, *J. Membr. Sci.*, **279**, 76 (2006).
18. J. Zou and W. Ho, *J. Membr. Sci.*, **286**, 310 (2006).
19. H. Matsuyama, K. Hirai and M. Teramoto, *J. Membr. Sci.*, **92**, 257 (1994).
20. S. Saedi, S. Madaeni, F. Seidi, A. Shamsabadi and S. Laki, *Chem. Eng. J.*, **236**, 263 (2014).
21. S. Saedi, S. Madaeni, F. Seidi, A. Shamsabadi and S. Laki, *Int. J. Greenh. Gas Control.*, **19**, 126 (2013).
22. S. Saedi, B. Nikravesh, F. Seidi, L. Moradi, A. Shamsabadi, M. Salarabadi and H. Salimi, *RSC Adv.*, **5**, 67299 (2015).
23. J. Albo, J. Wang and T. Tsuru, *J. Membr. Sci.*, **453**, 384 (2014).
24. Y. Zhang, C. Xiao, E. Liu, Q. Du and X. Wang, *Desalination*, **191**, 291 (2006).
25. L. Lianchao, W. Baoguo, T. Huimin, C. Tianlu and X. Jiping, *J. Membr. Sci.*, **269**, 84 (2006).
26. Y. Shepl, Y. Kotp, M. El-deab, H. Shawky and B. El-anadouli, *J. Membr. Sci.*, **391**, 215 (2012).
27. J. Kim, K. Lee and S. Youl, *J. Membr. Sci.*, **169**, 81 (2000).
28. Y. Zhang, N. E. Benes and R. G. H. Lammertink, *Lab. Chip.*, **15**, 575 (2015).
29. S. Sridhar, B. Smitha, S. Mayor, B. Prathab and T. Aminabhavi, *J. Mater. Sci.*, **42**, 9392 (2007).
30. Z. Zhang, F. Chen, M. Rezakazemi, W. Zhang, C. Lu, H. Chang and X. Quan, *Chem. Eng. Res. Des.*, **131**, 375 (2018).
31. Y. Mo, A. Tiraferri, N. Y. Yip, A. Adout, X. Huang and M. Elimelech, *Environ. Sci. Technol.*, **46**, 13253 (2012).
32. H. Rabiee, S. Meshkat and M. Soltanieh, *J. Ind. Eng. Chem.*, **27**, 223 (2015).
33. P. Jan, F. Detlev, K. Thomas and P. Klaus-viktor, *J. Membr. Sci.*, **389**, 343 (2012).
34. W. Lin, R. H. Vora and T. Chung, *J. Polym. Sci. Part B Polym. Phys.*, **38**, 2703 (2016).
35. F. Dorosti, M. Omidkhah and R. Abedini, *J. Nat. Gas Sci. Eng.*, **25**, 88 (2015).
36. S. C. Pesek and W. J. Koros, *J. Membr. Sci.*, **81**, 71 (1993).
37. M. A. Aroon, A. F. Ismail, M. M. Montazer-rahmati and T. Matsuura, *Sep. Purif. Technol.*, **72**, 194 (2010).
38. B. Chakrabarty, A. K. Ghoshal and M. K. Purkait, *J. Membr. Sci.*, **315**, 36 (2008).
39. R. M. Boom, I. M. Wlenk, T. Van and C. A. Smolders, *J. Membr. Sci.*, **73**, 277 (1992).
40. A. K. Ghosh, B. Jeong, X. Huang and E. M. V. Hoek, *J. Membr. Sci.*, **311**, 34 (2008).
41. F. Yuan, Z. Wang, S. Li, J. Wang and S. Wang, *J. Membr. Sci.*, **421**, 327 (2012).
42. S. D. Bruck, *Polymer*, **7**, 231 (1966).
43. Y. A. Shepl, Y. H. Kotp, M. S. El-deab, H. A. Shawky and B. E. El-anadouli, *J. Membr. Sci.*, **51**, 215 (2012).
44. K. C. Wong, P. S. Goh, B. C. Ng and A. F. Ismail, *RSC Adv.*, **5**, 31683 (2015).
45. W. Mcdanel, M. G. Cowan, N. O. Chisholm, D. L. Gin and R. D. Noble, *J. Membr. Sci.*, **492**, 303 (2015).
46. S. K. Sen and S. Banerjee, *J. Membr. Sci.*, **350**, 53 (2010).
47. D. Bera, P. Bandyopadhyay, S. Ghosh and S. Banerjee, *J. Membr. Sci.*, **453**, 175 (2014).
48. S. Banerjee, G. Maier, C. Dannenberg and J. Spinger, *J. Membr. Sci.*, **229**, 63 (2004).
49. X. Li, I. Kresse and Z. Xu, *Polymer*, **42**, 6801 (2001).
50. Q. Xin, H. Wu, Z. Jiang, Y. Li and S. Wang, *J. Membr. Sci.*, **467**, 23 (2014).
51. L. Ansaloni, Y. Zhao, B. T. Jung, K. Ramasubramanian, M. Giacinti and W. S. W. Ho, *J. Membr. Sci.*, **490**, 18 (2015).
52. A. Ebadi, M. Omidkhah and A. Kargari, *J. Membr. Sci.*, **490**, 364 (2015).

APPENDICES

Appendix A: Experimental Errors

There are two kinds of errors in the reported data: from the permeation measurements and from the membrane sample. To estimate the uncertainty of the reported measurements, the permeation of each gas was measured at least twice at the same condition on the same membrane sample. The error from the membranes sample was also estimated by preparing and testing at least

two independent different samples. The deviation of gas permeance and selectivity from the reported values are shown in Table A1 and A2. The data reported in this work are the average of the three measurements.

Table A1. Uncertainty in permeance-measurements for same polyamide membrane

T	CO_2	CH_4	N_2	O_2	CO_2/CH_4	CO_2/N_2	O_2/N_2
300.15	0.025	0.013	0.041	0.037	0.037	0.063	0.004
308.15	0.021	0.026	0.033	0.016	0.004	0.012	0.017
323.15	0.015	0.024	0.032	0.036	0.038	0.045	0.066

Table A2. Uncertainty in permeance due to membrane sample

T	CO_2	CH_4	N_2	O_2	CO_2/CH_4	CO_2/N_2	O_2/N_2
300.15	0.070	0.256	0.122	0.069	0.260	0.171	0.170
308.15	0.128	0.080	0.084	0.057	0.193	0.196	0.131
323.15	0.021	0.229	0.214	0.078	0.169	0.159	0.112